

# Fermi surface of CeIn<sub>3</sub> above the Néel critical field

N. Harrison<sup>1</sup>, S. E. Sebastian<sup>2</sup>, C. H. Mielke<sup>1</sup>, A. Paris<sup>1</sup>, M. J. Gordon<sup>1</sup>,  
C. A. Swenson<sup>1</sup>, D. G. Rickel<sup>1</sup>, M. D. Pacheco<sup>1</sup>, P. F. Ruminer<sup>1</sup>, J. B. Schillig<sup>1</sup>,  
J. R. Sims<sup>1</sup>, A. H. Lacerda<sup>1</sup>, M.-T. Suzuki<sup>3</sup>, H. Harima<sup>3</sup>, and T. Ebihara<sup>4</sup>

<sup>1</sup>*National High Magnetic Field Laboratory, Los Alamos National Laboratory, MS E536, Los Alamos, New Mexico 87545*

<sup>2</sup>*Cavendish Laboratory, University of Cambridge, Madingley Road, Cambridge CB3 0HE, UK*

<sup>3</sup>*Department of Physics, Kobe University, Kobe 657-8501, Japan*

<sup>4</sup>*Department of Physics, Shizuoka University, Shizuoka 422-8529, Japan*

(Dated: February 1, 2008)

We report measurements of the de Haas-van Alphen effect in CeIn<sub>3</sub> in magnetic fields extending to  $\approx 90$  T, well above the Néel critical field of  $\mu_0 H_c \approx 61$  T. The unreconstructed Fermi surface sheet is observed in the high magnetic field polarized paramagnetic limit, but with its effective mass and Fermi surface volume strongly reduced in size compared to that observed in the low magnetic field paramagnetic regime under pressure. The spheroidal topology of this sheet provides an ideal realization of the transformation from a ‘large Fermi surface’ accommodating  $f$ -electrons to a ‘small Fermi surface’ when the  $f$ -electron moments become polarized.

Strong magnetic fields are an indispensable tool for studying the energy scales relevant to antiferromagnetism. By polarizing their magnetic moments, they deplete the system of available spin degrees of freedom for staggered ordering. In  $f$ -electron antiferromagnets, polarization is expected to be accompanied by the effective removal of the  $f$ -electron degrees of freedom from the Fermi surface (FS) [1, 2, 3], enabling access to the underlying electronic structure in its simplest form. The  $f$ -electron system CeIn<sub>3</sub> provides an essential paradigm to understand universal aspects of the relationship between antiferromagnetism and unconventional superconductivity—given the magnetic simplicity of this non-metamagnetic cubic system [2, 4] compared to CeRu<sub>2</sub>Si<sub>2</sub> [5], CeB<sub>6</sub> [6] or CeRhIn<sub>5</sub> [7] due to the absence of metamagnetism. Universal behavior is realized in CeIn<sub>3</sub> by the application of pressure, whereupon antiferromagnetism is suppressed and superconductivity [8] and a heavy fermion behavior emerge [9]. If NdB<sub>6</sub> provides a model example of a cubic system in which the hybridization between the  $f$ -electrons and conduction electrons remains negligible throughout [10], then CeIn<sub>3</sub> may be considered as the model system for understanding antiferromagnetism preceding superconductivity in the opposite strongly correlated regime comprising heavy quasiparticles [11, 12].

One unavoidable consequence of a monotonic non-metamagnet magnetization is that much stronger magnetic fields are required to polarize the quasiparticle bands to suppress the correlations [13, 14]. In CeIn<sub>3</sub> this requires exceeding the critical field of the Néel ordered phase,  $\mu_0 H_c \approx 61$  T [4]. To determine the electronic structure of CeIn<sub>3</sub> in magnetic fields above  $H_c$ , we utilize the recently constructed 100 tesla magnet at Los Alamos [15]—presently delivering magnetic fields of up to 90 T (see Fig. 1) while being commissioned. Measurements of the de Haas-van Alphen (dHvA) effect over a wide interval in field above  $H_c$  enable the unrecon-

structed FS of CeIn<sub>3</sub> to be observed in the polarized state, and compared with that previously observed in the paramagnetic regime at pressures exceeding the critical pressure  $p_c \approx 26$  kbar [9].

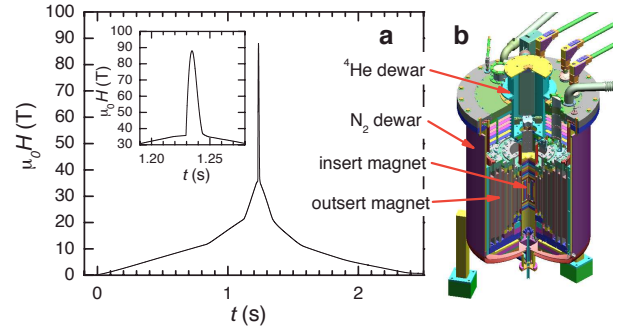


FIG. 1: **a** The  $H$ -versus-time  $T$  profile of the pulse generated by the combined ‘outsert’ and ‘insert’ magnets. The inset shows the region of the pulse profile provided by the insert magnet in which dHvA measurements in Fig. 2 are made. **b** A schematic of the magnet used for generating the pulse (outer diameter  $\approx 1.4$  m).

The magnetic field  $\mathbf{H}$  is generated in two stages. First, a 1.4 GW motor-generator is used to energize an ‘outsert’ coil, delivering a  $\approx 36$  T ‘base’ magnetic field in a 0.2 m bore. A 2.5 MJ capacitor bank is then used to energize an ‘insert’ coil to produce the remaining  $\approx 54$  T in a 15 mm bore [16]. Figure 1a shows an example of the total magnetic field-versus-time profile experienced by the CeIn<sub>3</sub> samples studied in this work. With the exception of the magnetic field generation, the dHvA experimental technique is identical to that used in regular pulsed magnetic field experiments [4, 10, 21]. Three single crystalline CeIn<sub>3</sub> samples are cut and etched to diameters of less than  $300 \mu\text{m}$  for experiments with  $\mathbf{H} \parallel \langle 100 \rangle$ ,  $\langle 110 \rangle$  and  $\langle 111 \rangle$ . The dHvA effect is measured using a coaxially-arranged compensated pair of detection coils

with the innermost coil having  $\approx 460$  turns and an inner bore of  $450 \mu\text{m}$ . A digitizer captures the dHvA signal data while temperatures between 300 mK and 4 K are obtained by controlling the vapor pressure of liquid  $^3\text{He}$  and  $^4\text{He}$  reservoirs.

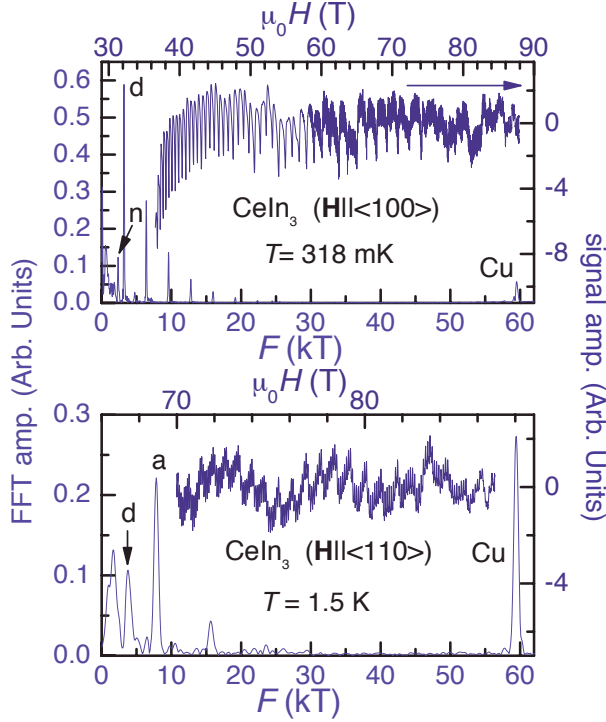


FIG. 2: Examples of dHvA signal measurements on  $\text{CeIn}_3$  for two different orientations of  $\mathbf{H}$  together with Fourier transformations. The Cu signal originates from the polycrystalline Cu comprising the detection coils.

Figure 2 shows examples of dHvA signals and Fourier transforms for  $\mathbf{H} \parallel \langle 100 \rangle$  and  $\langle 110 \rangle$ . For  $\mathbf{H} \parallel \langle 100 \rangle$ , the signal is dominated by the d-branch in both the antiferromagnetic ( $\mu_0 H < \mu_0 H_c \approx 61 \text{ T}$ ) and polarized paramagnetic regimes ( $H > H_c$ ). The n-frequency [11] is also observed to appear prominently at high magnetic fields. The a-sheet (see Fig. 3) yields a relatively weak feature corresponding to a large electron sheet centered at the R point of the Brillouin zone [17]; observable above the level of noise over a restricted interval 75-85 T in magnetic fields (see Fig. 3). This frequency becomes more prominent for  $\mathbf{H} \parallel \langle 110 \rangle$  (Fig. 2, lower panel) and  $\langle 111 \rangle$ , appearing at all fields  $\mu_0 H \gtrsim 55 \text{ T}$ .

Fermi surface measurements of Ce compounds are often reported to be consistent with either of two dichotomous scenarios. In one scenario, good agreement is found with bandstructure calculations in which the  $f$ -electron shells are completely filled or empty, as for the Lu and La analog compounds, indicating that the  $f$ -electrons contribute negligibly to the FS volume. A compound with these characteristics is considered to have a ‘small FS’

(i.e. the FS is much smaller than it might otherwise be were the  $f$ -electrons to contribute their charge degrees of freedom) [18]. In the other scenario, some level of agreement is found with bandstructure calculations in which the  $f$ -electrons are treated as band electrons. A compound with these characteristics is then considered to have a ‘large FS’ (see Fig. 4) [18]. Our present measurements outside the antiferromagnetic phase of  $\text{CeIn}_3$  reveal that both these scenarios are realized in the same isotropic material under conditions of either extreme pressure [9] or intense magnetic field. dHvA measurements made at  $p > p_c$  are consistent with band structure calculations in which the  $f$ -electrons are treated as itinerant, as shown in Fig. 3 [17]. Satisfactory agreement requires the effects of Coulomb repulsion and the orbital manifold of the lowest lying  $\Gamma_7$  doublet to be taken into consideration [17]. Our high magnetic field a-sheet measurements on  $\text{CeIn}_3$  (see Fig. 3), in contrast, are found to be similar to the predicted electronic structure of  $\text{LuIn}_3$ , which has filled  $f$ -shells.  $\text{CeIn}_3$  therefore provides a particularly clear example of a system in which a transformation occurs from a ‘large FS’ at high pressures and low magnetic fields to a ‘small FS’ at high magnetic fields and ambient pressure. Since  $\text{CeIn}_3$  is non-metamagnetic [2, 4] and it is possible (in principle) to move from the high pressure regime to the high magnetic field regime without crossing the antiferromagnetic phase boundary, the transformation in FS must take place in a continuous fashion.

The present experimental limitations require us to study the link between the high pressure and high magnetic field regimes via the intervening antiferromagnetic phase. The manner in which each section of the FS is modified by the antiferromagnetic order parameter depends on its size, location in  $\mathbf{k}$  space and the extent to which it accommodates  $f$ -electrons. The d-sheet passes through  $H_c$  and  $p_c$  in Fig. 4 relatively unperturbed in topology or effective mass [9, 17] as indicated in Figs. 2 and 5a. This robustness to antiferromagnetism and high magnetic fields arises from the minimal contribution of the  $f$ -electrons to the d-sheet volume (the  $f$ -electron dispersion exhibits a deep minimum at the  $\Gamma$  point in the Brillouin zone [17]), and its small size well within the interior of the antiferromagnetic Brillouin zone.

The a-sheet, by contrast, is radically affected by antiferromagnetism owing to its much greater size and hybridization with the  $f$ -dispersion near the Fermi energy. The large size of the staggered moment within the antiferromagnetic phase of  $\text{CeIn}_3$  [19], combined with the weak dispersion of the  $f$ -band in the paramagnetic phase [17], requires the antiferromagnetism to be considered from the strong coupling perspective [12]. The disappearance of the a-sheet at pressures  $p < p_c$  [9] reflects the effective removal of the majority of the  $f$ -electrons from the FS deep within the antiferromagnetic phase, where strong coupling gaps the  $f$ -electron dispersion. Unlike

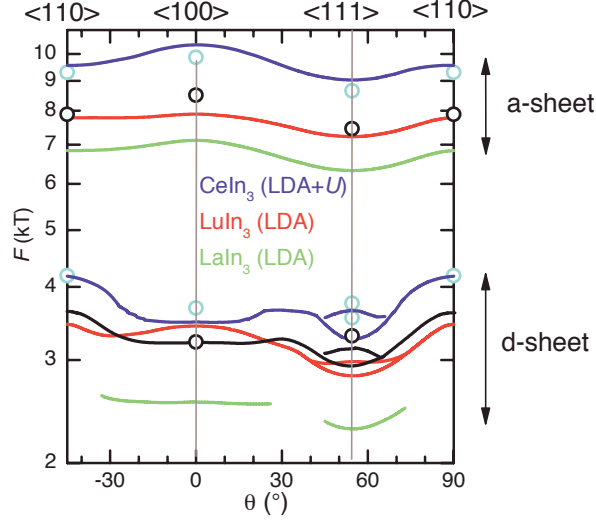


FIG. 3: A comparison of the d- and a-sheet FS's of  $\text{CeIn}_3$  measured at ambient pressure and 27 kbar with those calculated for  $\text{CeIn}_3$  (blue lines),  $\text{LuIn}_3$  (red lines) and  $\text{LaIn}_3$  (green lines) using the local density approximation (LDA) method (inclusive of the Coulomb interaction  $U$  in the case of  $\text{CeIn}_3$  [17]). Black lines indicate the magnetic field-orientation dependence of the d-sheet obtained by Endo *et al* [11], revealing a close similarity to that of  $\text{LuIn}_3$ . Measured frequencies are constant to within 1 % between 50 and 90 T. Black open circles represent the a- and d-sheets observed by us in strong magnetic fields and ambient pressure, while cyan circles represent the d- and a-sheets measured by Settai *et al.* for  $p > p_c$  [9].

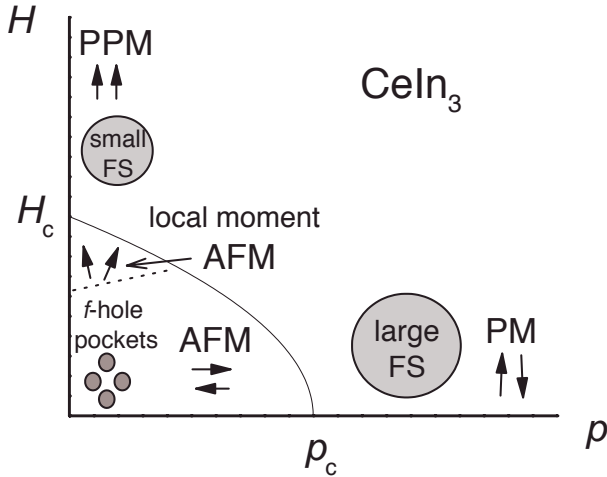


FIG. 4: A schematic  $p$  versus  $H$  phase diagram of  $\text{CeIn}_3$ , including the antiferromagnetic (AFM), paramagnetic (PM) and polarized paramagnetic (PPM) regimes. Solid arrows represent the spin states of the  $\Gamma_7$  doublet of Ce in each of these regimes, while the grey circles represent the different FS's. The 'large FS' includes  $f$ -electron charge degrees of freedom whereas the 'small FS' does not. Small  $f$ -hole pockets have recently been observed inside the antiferromagnetic phase at ambient pressure [12], but are observed to become depopulated in magnetic fields above  $\approx 41$  T (dotted line) where the staggered moment is canted.

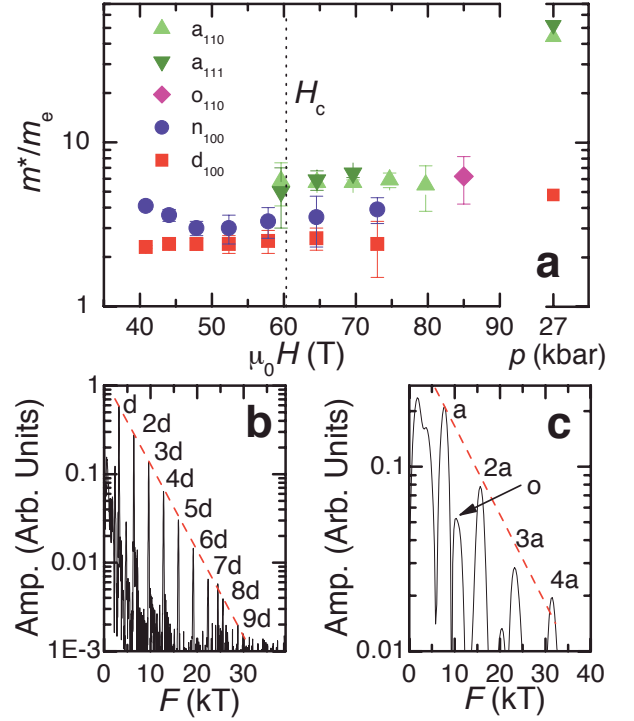


FIG. 5: **a** Effective masses of different extremal dHvA orbits in  $\text{CeIn}_3$ , estimated by fitting the Lifshitz-Kosevich theoretic form to the temperature dependence of the quantum oscillation amplitude measured between 300 mK and 4 K. The subscript in the legend refers to the orientation of  $\mathbf{H}$ . Masses for the same orbits measured at  $p > p_c$  by Settai *et al.* are shown to the right for comparison. **b** Part of the  $\mathbf{H} \parallel \langle 100 \rangle$  Fourier transform from Fig. 2 plotted on a logarithmic scale so as to show the exponential dependence of the  $d_{100}$  frequency harmonics on harmonic index. The red dotted line is a guide to the eye. **c** A similar Fourier transform for the  $a_{110}$  frequency, performed over a restricted interval in magnetic field 80-87 T where the harmonic content is most pronounced.

the d-sheet FS, the evolution of the a-sheet FS topology cannot easily be predicted in the intermediate regime close to the antiferromagnetic boundary where local staggered moment ordering competes with Kondo screening [20]. A clearer picture begins to emerge in high magnetic fields once the hybridization becomes perturbatively weak due to the field-induced polarization of the quasiparticle bands (as with the suppression of Kondo screening deep within the antiferromagnetic phase [12]). The effective mass of the a-sheet in Fig. 5a is observed to be magnetic field independent (within experimental error) and roughly an order of magnitude smaller than that observed at  $p > p_c$ , providing a compelling evidence for the removal of the majority of the  $f$ -electrons from this sheet due to the field-induced polarization of the quasiparticle bands [3]. Whilst the experimental picture at low magnetic fields and ambient pressure is more complex, with small pockets of  $f$ -holes [12] coexisting with

fragments of the unhybridized conduction band FS resembling  $\text{LuIn}_3$ , magnetic breakdown tunneling at higher magnetic fields causes the re-emergence of this a-sheet at fields slightly below  $H_c$ .

Spin-dependent effective masses are another consequence of the polarization of the  $f$ -electrons in strong magnetic fields. In the case of the  $d_{100}$  frequency, shown in Fig. 5b, the absence of a significant  $f$ -electron contribution causes the spin dependence to closely mimic the localized  $f$ -electron behavior seen in the single impurity limit, as realized in  $\text{Ce}_x\text{La}_{1-x}\text{B}_6$  [21] and  $\text{Ce}_x\text{La}_{1-x}\text{RhIn}_5$  [22] for  $x \lesssim 10\%$ . Localization of the  $f$ -electrons causes the spin-up and -down dHvA frequencies to be the same, but with the lighter mass spin component dominating the dHvA frequency, causing the harmonic index-dependence of the dHvA amplitude to decay in a simple exponential manner. In the case of the  $a_{110}$  frequency, four harmonics are observed at the highest magnetic fields,  $80 < \mu_0 H < 87$  T, in Fig. 5c. The observed field-independence of the a-sheet FS topology and effective mass suggests that the polarization of the quasiparticle bands is more complete than realized in  $\text{CeB}_6$  and  $\text{CeRu}_2\text{Si}_2$ , where well separated dHvA frequencies corresponding to split spin-up and -down Fermi surfaces and/or field-dependent effective masses are observed [5, 23]. Exchange splitting effects caused by the polarized  $f$ -moments (as in  $\text{NdB}_6$  [10, 24]) can also not be resolved at high magnetic fields in  $\text{CeIn}_3$ . The new  $o_{110}$  frequency (and its harmonic) at  $\approx 10400$  T in Fig. 5c has a similar size to other features predicted in the  $\text{LuIn}_3$  bandstructure calculations [25].

In summary, we observe the a-sheet FS of  $\text{CeIn}_3$  in strong magnetic fields  $H > H_c$ , which is found to be consistent with the ‘small FS’ picture [18], in which the  $f$ -electrons do not contribute significantly to its volume, in contrast to that observed within the paramagnetic regime at pressures  $p > p_c$ . Consequently, its effective mass is observed to be reduced by an order of magnitude compared to that at  $p > p_c$ . The spheroidal geometry of the FS represents an ideal embodiment of the change in the electronic structure from large FS (at high pressure) to a small FS (in strong magnetic fields). Although a direct observation of this transformation is presently masked by the intervening antiferromagnetic phase, the transformation is expected to take place continuously given the cubic symmetry of  $\text{CeIn}_3$  [2] (the absence of metamagnetism is already established at ambient pressure [4]). The present experiments on  $\text{CeIn}_3$  show the importance of extreme experimental conditions for understanding electronic structure of strongly correlated  $f$ -electron metals.

This work was performed under the auspices of the National Science Foundation, the Department of Energy (US) and Florida state. T.E. acknowledges support provided by Grant-in-Aid for Scientific Research on priority

Areas, ‘High Field Spin Science in 100T’ (CASIO) and MEXT. S.E.S. acknowledges support from the Institute for Complex Adaptive Matter and from Trinity College, Cambridge University.

- 
- [1] A. Wasserman, M. Springford and A. C. Hewson, *J. Phys.: Cond. Matt.* **1**, 2669 (1989).
  - [2] S. M. M. Evans, *Europhys. Lett.* **17** 469 (1992).
  - [3] D M. Edwards and A. C. M. Green, *Z. Phys. B* **103**, 243 (1997).
  - [4] T. Ebihara *et al.*, *Phys. Rev. Lett.* **93**, 246401 (2004).
  - [5] Strong anisotropy of the hybridization between the  $f$ -electrons and the conduction electrons is required to explain metamagnetism in  $\text{CeRu}_2\text{Si}_2$  in the absence of magnetic ordering [2].
  - [6] Metamagnetism in  $\text{CeB}_6$  is caused by a transition between antiferromagnetic and antiferroquadrupolar phases (otherwise unexpected in a cubic system [2]); R. G. Goodrich *et al.*, *Phys. Rev. B* **69**, 54415 (2004).
  - [7] The upper critical field of the antiferromagnetic phase of  $\text{CeRhIn}_5$  appears to coincide with metamagnetism, possibly as a consequence of the anisotropy of the crystal electric fields in the tetragonal symmetry; T. Takeuchi *et al.*, *J. Phys. Soc. Japan* **70**, 877 (2001).
  - [8] N. D. Mathur *et al.*, *Nature* **394**, 39 (1998).
  - [9] R. Settai *et al.*, *J. Phys. Soc. Japan* **74**, 3016 (2005).
  - [10] R. G. Goodrich, N. Harrison and Z. Fisk, *Phys. Rev. Lett.* **97**, 146404 (2006).
  - [11] M. Endo, N. Kimura and H. Aoki, *J. Phys. Soc. Japan* **74**, 3295 (2005).
  - [12] S. E. Sebastian *et al.* (unpublished); Effective masses as large as 100 times the free electron mass  $m_e$  are observed in fields approaching  $\approx 41$  T.
  - [13] J. A. Detwiler *et al.*, *Phys. Rev. B* **61**, 402 (2000).
  - [14] T. Sakakibara *et al.*, *J. Magn. Magn. Mater.* **70**, 375 (1987).
  - [15] J. L. Bacon *et al.*, *IEEE Trans. Appl. Supercon.* **12**, 695 (2002).
  - [16] C. A. Swenson *et al.*, *Physica B* **346-347**, 561 (2004).
  - [17] M.-T. Suzuki, (Ph. D thesis, Kobe University, 2007); M.-T. Suzuki and H. Harima (submitted to SCES, Houston, 2007, to appear in *Physica B*).
  - [18] P. Coleman *et al.*, *J. Phys.: Cond. Matt.* **13**, R723 (2001).
  - [19] J. M. Lawrence, and S. M. Shapiro, *Phys. Rev. B* **22** 4379 (1980).
  - [20] Q. M. Si, *Physica B* **378**, 23 (2006).
  - [21] N. Harrison *et al.*, *Phys. Rev. Lett.* **81**, 870 (1998); A. A. Teklu *et al.*, *Phys. Rev. B* **62**, 12875 (2000).
  - [22] U. Alver *et al.*, *Phys. Rev. B* **64**, 180402 (2001).
  - [23] Evidenced by recent observations of a new frequency  $\alpha'$ , smaller and heavier than that of the  $\alpha_1$  frequency, but corresponding to the same topology, as revealed by its angular dependence; M. Endo *et al.*, *J. Phys. Soc. Japan* **75**, 114704 (2006).
  - [24] L. P. Gor'kov and P. D. Grigoriev, *Phys. Rev. B* **73**, 060401 (2006).
  - [25] H. Harima (private communication).